Angular distribution of hot electrons incident on a laser-irradiated target

J. C. Kieffer, J. P. Matte, and H. Pépin
Institut National de la Recherche Scientifique—Energie, Université du Québec, Varennes, Québec J0L 2P0, Canada

R. Decoste
Institut de Recherche d'Hydro—Québec, Varennes, Québec J0L 2P0, Canada
(Received 28 June 1983)

Angular distributions of bremsstrahlung emission are calculated for various energy and angular distributions of hot electrons incident on a laser-irradiated plastic target. These theoretical results are used to interpret experimental data of x-ray continuum emission from a CO_2-laser-produced plasma. It is shown that at low irradiance ($I_L \leq 5\times 10^{12}$ W/cm^2) the incident electrons are normal to the target surface but that at higher irradiance, the incident electrons' angular distribution (spatially integrated over the target surface) is semi-isotropic. The influence of the directional distribution of hot electrons on axial energy transport is also studied by comparing calculated continuum x-ray spectra as well as energy-deposition profiles with experimental results.

I. INTRODUCTION

In laser-matter interaction, energetic electrons are generated mainly by resonance absorption at the critical density surface and also possibly by parametric decay processes. These hot electrons are emitted predominantly into the corona, but space-charge electric fields draw them back into the target. Hot electrons have been the subject of extensive studies[1–8] because their presence strongly influences the design and the performances of laser fusion targets. Ultimately, all these studies aim at determining and controlling the energy dissipated by the hot electrons at various locations in the solid material. The knowledge of the energy dissipation rate requires a determination of both the energy and the directional distribution of the incident hot electrons. Moreover, recent theoretical[9] and experimental results[10,11] have shown the influence of self-generated magnetic fields[12] on hot-electron trajectories and consequently on energy transport. It is then particularly important to study directly the angular distribution of hot electrons incident on a laser-irradiated target. This paper presents a detailed analysis of the direction of incidence of hot electrons under various irradiance conditions and shows that the energy-deposition characteristics are strongly dependent on the directional distribution of hot electrons.

In this paper, the directions of incidence of suprathermal electrons going into the solid target are inferred from bremsstrahlung emission. Several experimental studies[13] have already investigated the intensity isotropy of hard-x-ray bremsstrahlung. However, when significant anisotropy of intensity was measured, there was no detailed interpretation of this effect in terms of the directional distribution of incident hot electrons. Theoretical anisotropies in a laser-produced plasma have also been calculated,[14] but this has been done for electrons at normal incidence only and in the nonrelativistic approximation. In this paper, we calculate bremsstrahlung angular distributions obtained for various energy and directional distributions of electrons incident on a plastic target. We take into account retardation and relativistic effects[15] since the nonrelativistic approximation severely deforms the angular distribution, even for electron energies as low as 10 keV. We present detailed calculations for the thin-target case and apply the analysis to the thick-target case. We are then able to consistently interpret measurements of x-ray intensity anisotropy.

In Sec. II of this paper we describe the experimental arrangement which has been used to study the directions of incidence of hot electrons and the electron penetration into the solid target. Section III gives the theoretical bremsstrahlung angular distributions which enable us to interpret experimental results of x-ray continuum emission from a CO_2-laser-produced plasma and to determine the direction of incidence of hot electrons under various irradiance conditions. Section IV shows the influence of the hot electrons' angular distributions on the axial energy deposition. The axial energy-deposition features are inferred from the hard-x-ray continuum emitted from a high-Z tracing material covered with a plastic layer of variable thickness. Finally, conclusions are presented in Sec. V.

II. EXPERIMENTAL ARRANGEMENT

The experimental study is carried out with a CO_2-laser facility delivering 50 J in a 1.2-ns full width at half maximum (FWHM) pulse. The laser beam, incident at 28°, is focused onto the target by an $f/1.5$ off-axis parabolic mirror. At best focus, 50% of the energy is contained within a 120-μm-diam spot. The experiments are made at energy levels up to 15 J corresponding to a maximum irradiance of 6×10^{13} W/cm^2. The time- and space-integrated continuum x-ray emission is recorded with nine K-edge filter detectors covering the 1—70-keV range.[16] The angular x-ray distribution is obtained by using four detectors at vari-

ous polar and azimuthal angles to measure the hard-x-ray emission of thick plastic targets. Spatially resolved x-ray spectra are obtained from the local hard-x-ray emission detected with high-Z tracing material techniques. The targets are composed of plastic films of various thicknesses deposited on a thick gold substrate; the inward resolution is obtained by measuring the substrate hard-x-ray continuum emitted by hot electrons after deceleration in the plastic layer.

III. BREMSSTRAHLUNG ANGULAR DISTRIBUTION

In this section we first calculate continuum x-ray angular distributions which are directly related to the direction of incidence of electrons. Then we use the theoretical results for the interpretation of measured x-ray angular distributions.

A. Monoenergetic electrons

Highly elaborate computations of emission due to single-electron—ion collisions, including all relativistic effects and screening due to atomic electrons, have been recently performed.[17,18] In the present work, we will use an expression of x-ray emission taken from Ref. 19, which is valid for pure Coulomb fields and moderate electron energies. The angular x-ray distribution thus obtained for monoenergetic electrons is shown to be in very good agreement with theoretical[18] and experimental[20] results for intermediate electron energies ($\lesssim 200$ keV).

Consider an electron of velocity v_1 and energy E_1, which collides with an ion at rest of charge Ze. The electron is incident in the positive z direction. A photon of energy $h\nu$ is emitted at an angle θ with respect to the direction of the incident electron; the outgoing electron has velocity v_2 and energy E_2. We have

$$E_1 = mc^2(1-\beta_1^2)^{-1/2} = h\nu + E_2 = h\nu + mc^2(1-\beta_2^2)^{-1/2} ,$$

where $\beta_{1,2} = v_{1,2}/c$.

The expression for the emitted intensity is[19]

$$I_1(\theta,h\nu,E_1) = I_x \frac{(1-\beta_1^2)\sin^2\theta}{(1-\beta_1\cos\theta)^4} + \frac{I_y}{(1-\beta_1\cos\theta)^2}\left[2 - \frac{(1-\beta_1^2)\sin^2\theta}{(1-\beta_1\cos\theta)^2}\right] , \quad (1)$$

where I_x and I_y involve integrations over all angles of the outgoing electron waves.[21] The intensity I_1 defined as $\Delta P/j\Delta\nu\Delta\Omega$ is the power ΔP radiated into the solid angle $\Delta\Omega$ and in the frequency interval $\Delta\nu$ for an electron current of density j bombarding an ion, and is expressed in erg s cm^2/sr. The intensities I_x and I_y are calculated as in the nonrelativistic case,[21,22] but they are multiplied by the factor[22] $\gamma^{-4} = (1-\beta^2)^2$. This factor permits us to avoid large overestimates[17,22] of the emission which results from merely including the retardation correction. Integration of Eq. (1) over emission angles gives (in erg s cm^2)

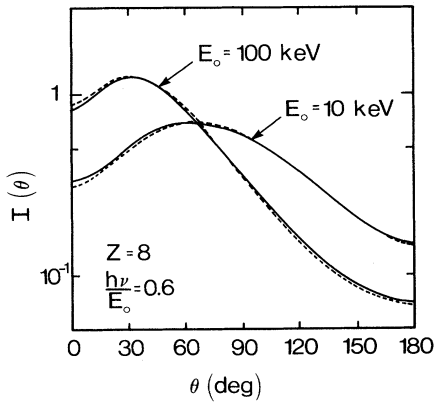

FIG. 1. Comparison of angular x-ray distributions obtained from Eq. (1) (solid line) and results of Ref. 18 (dashed line) for $Z=8$ and electron energies of 10 and 100 keV. Values $I(\theta)$ are normalized such that $\int_0^\pi I(\theta)\sin\theta\, d\theta = 1$.

$$I_2(h\nu,E_1) = \tfrac{8}{3}\pi(1-\beta_1^2)^{-1}(I_x + 2I_y) . \quad (2)$$

The angular x-ray distribution obtained from (1) is compared in Fig. 1 to more elaborate calculations of Tseng *et al.*[18] for $Z=8$ and for electron energies of 10 and 100 keV. Clearly, it appears that for low-Z materials and for intermediate energies, we obtain a very good agreement. In Table I, we see that the results of Eq. (1) are very close to the experimental values of Rester *et al.*[20] on aluminum. We will now use this model to calculate the emission for incident electrons with various energy and angular distributions.

B. Incident electrons with various energy and angular electron distributions

We consider an electron of velocity v_1 and energy E_1 impinging in the direction θ',ϕ' on an ion; a detector in the direction θ'',ϕ'' will receive an intensity $I_1(\theta,h\nu,E_1)$, given by Eq. (1), where θ is the angle between the two directions (see Fig. 2) such that

$$\cos\theta = \cos(\phi'-\phi'')\sin\theta'\sin\theta'' + \cos\theta'\cos\theta'' .$$

We assume that the electron distribution is the product of an energy distribution and a directional distribution:

$$F(E_1,\theta') = f(E_1)g(\theta') . \quad (3)$$

TABLE I. Comparison of data from Ref. 20 and calculations for aluminum (values of $(k/Z^2)d^2\sigma/dk\,d\Omega$ where $k=2\pi\nu/c$ are obtained after dividing $I_1(\theta,h\nu,E_1)$ [Eq. (1)] by $6.63\times10^{-54}Z^2$).

θ (deg)	Ref. 20	$\frac{k}{Z^2}\frac{d^2\sigma}{dk\,d\Omega}$
20	5.3	5.3
30	5.2	5.5
40	4.8	5.4
60	4.2	4.5
120	1.6	1.5

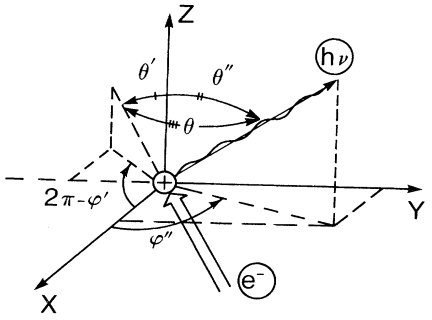

FIG. 2. Definition of coordinates. Angles θ' and ϕ' give the direction of electron incidence on the ion. Angles θ'' and ϕ'' determine the direction of observation.

We also assume the azimuthal symmetry.

The normalizations expressions are

$$\int_0^\infty f(E_1)dE_1=1 , \tag{4a}$$

$$2\pi\int_0^\pi g(\theta')\sin\theta' d\theta'=1 . \tag{4b}$$

The energy distribution is taken to be of the form

$$f(E_1)=AE_1^n\exp(-E_1/kT_e) , \tag{5}$$

where T_e is the electron temperature and n the parameter characterizing the distribution.

We consider electrons incident along directions θ' such that $0\le\theta'\le\theta_2$, and we write the directional distributions as follows:

$$g(\theta')=\begin{cases}B=\text{const}, & \theta'\le\theta_2\\ 0, & \theta'\ge\theta_2\end{cases} \tag{6}$$

where B is chosen to satisfy the normalization condition in Eq. (4). The values $\theta_2=0°$, 90°, and 180° mean, respectively, a monodirectional, a semi-isotropic, and an isotropic distribution. When electrons are all incident at the same angle θ_2 with respect to the z direction one has

$$g(\theta')=\delta(\theta'-\theta_2)/2\pi\sin\theta_2 . \tag{7}$$

The intensity emitted, per electron, by the distribution given by Eq. (3) is then (in erg/sr)

$$I(T_e\theta'',h\nu)=2\int_{h\nu}^\infty v_1 f(E_1)dE_1\int_0^{\theta_2} g(\theta')\sin\theta' d\theta' \times\int_0^\pi I_1(\theta,h\nu,E_1)d\phi' . \tag{8}$$

Angular distributions of x-ray emission obtained for a monodirectional electron distribution incident in the z direction ($\theta_2=0$) are shown in Fig. 3 (for a given temperature and various frequencies) and in Fig. 4 (for a given emission frequency, and different temperatures). Changing n has little effect on the angular distribution (Fig. 3), but a considerable effect on the absolute intensity (Fig. 5). We must note that the x-ray angular distribution is practically independent of Z for low Z (≤ 20); but, of course, the absolute intensity varies approximately as Z^2.

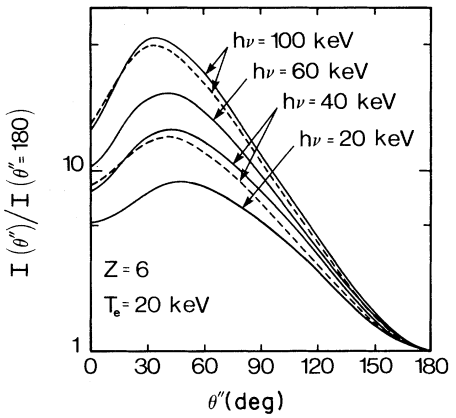

FIG. 3. Normalized angular x-ray distributions for various emission frequencies, the electron distribution being monodirectional. Solid lines correspond to the case $n=-\frac{1}{2}$ and the dashed lines to $n=\frac{1}{2}$.

Figure 6 presents the x-ray angular distribution obtained for various θ_2 angles, the electron angular distribution being given by Eq. (6). We see that the anisotropy, defined as the ratio $I(\theta'')/I(180°)$ for any value of θ'', decreases when θ_2 increases. It is verified for $\theta_2=180°$ (isotropic distribution), that we obtain an isotropic bremsstrahlung emission. Since the curves are normalized to the $\theta''=180°$ emission, the absolute values for $\theta''=180°$ are given in Table II. Figure 7 shows the variation of the angular distribution, calculated for $kT_e=20$ keV and $\theta_2=90°$ (semi-isotropic distribution), with the emission frequency. The normalization values ($\theta''=180°$) appear in Table III. Figure 8 gives the x-ray angular distributions obtained when electrons are all incident at 45° with respect to the z direction. The curves are normalized to $\theta''=180°$ and the absolute values at this angle are given in Table IV.

A comparison of Figs. 3, 7, and 8 shows clearly that the x-ray angular distribution is very sensitive to the direction of incidence of electrons. The calculations which have been presented can be directly applied to thin targets. We will show in Sec. III C that they also can be used to analyze low-Z thick-target results.

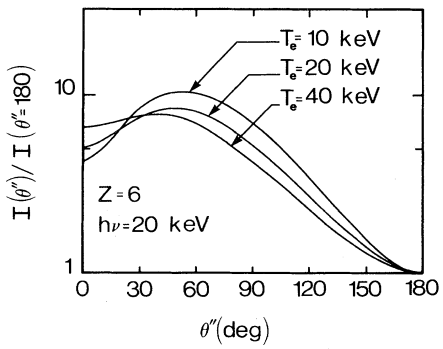

FIG. 4. Normalized angular x-ray distributions for various hot-electron temperatures. Electron distribution is monodirectional with $n=-\frac{1}{2}$.

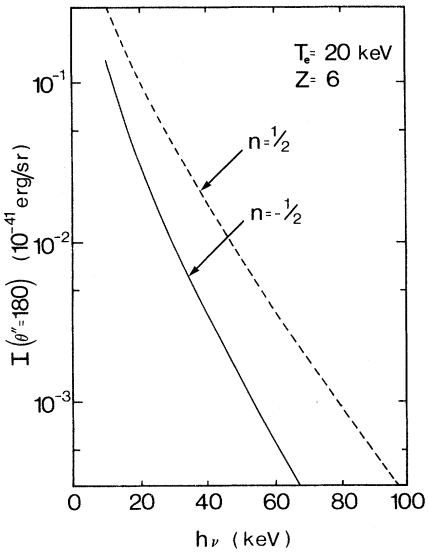

FIG. 5. X-ray spectra obtained at $\theta''=180°$ for a monodirectional electron distribution. Solid and dashed lines correspond to the case $n=-\frac{1}{2}$ and $\frac{1}{2}$, respectively.

C. Thick-target case

In a thick target, electrons undergo elastic and inelastic collisions causing angular scattering and energy losses. Because of these effects, the thick-target x-ray angular distribution cannot, in the general case, be easily related to thin-target results. However, for a low-Z target, it is possible to estimate these effects in a simple manner, since the x-ray continuum emission is mostly produced by electrons which have linear trajectories in the matter and since backscattering is negligible.[23]

In plastic, electrons having a range R are in a diffusive regime[24] after a length $x_D=0.7R$. The electrons which pass from their initial energy to an energy $h\nu$ in a length $s \leq x_D$ will contribute to the x-ray emission at $h\nu$ in the linear part of their trajectories. We can estimate, for the angular integrated x-ray emission of a thick low-Z target, the contribution to the total emission at a given energy $h\nu$ of electrons having not yet reached the diffusive regime.[25] For instance, for an electron energy distribution given by Eq. (5) with normal incidence and $kT_e=20$ keV, we find that electrons having linear trajectories in the plastic produce 70% of the x-ray emission at $h\nu=30$ keV; 30% of this emission comes from electrons which have undergone large-angle or multiple small-angle collisions and which have, consequently, an isotropic distribution in the material.

TABLE II. X-ray emission intensities at $\theta''=180°$ for electrons having directions of incidence in various cone angles θ_2 ($T_e=20$ keV, $h\nu=40$ keV, $n=\frac{1}{2}$).

θ_2 (deg)	$I(\theta''=180°)$ (erg/sr)
0	1.725×10^{-43}
30	2.073×10^{-43}
45	2.541×10^{-43}
60	3.258×10^{-43}
90	5.652×10^{-43}

We can use these results to estimate a lower limit to the x-ray anisotropy obtained with a thick plastic material. For this purpose, we add the following two contributions, with appropriate weighting factors obtained from thick target calculations integrated over all angles: (i) the angular emission from the incident energy distribution with electrons having linear trajectories, assuming negligible electron losses and (ii) the angular emission from the same incident energy distribution with an isotropic angular distribution of electron and also negligible electron losses. We find that the lower limit to the x-ray anisotropy in the thick-target case remains close to what is directly obtained with thin targets, in agreement with recent experimental results of low-Z targets irradiated by monoenergetic electrons.[26]

In Sec. III D the theoretical predictions of the x-ray angular distribution from a thick target are represented by a zone included between two theoretical curves, one being the thin-target calculation result, the other being the lower limit of the thick-target case as obtained above.

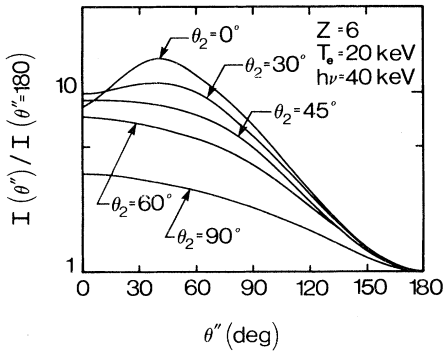

FIG. 6. Normalized angular x-ray distributions for electrons having directions of incidence in various cone angles θ_2 ($h\nu=40$ keV, $T_e=20$ keV, $n=\frac{1}{2}$).

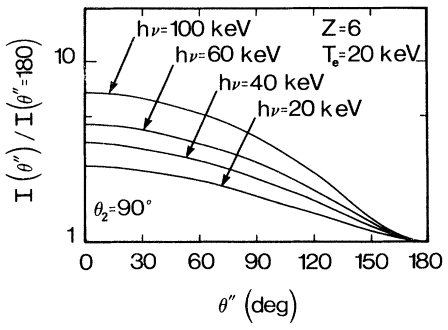

FIG. 7. Normalized angular x-ray distributions for various emission frequencies. Electron distribution is now semi-isotropic ($\theta_2=90°$, $T_e=20$ keV, $n=\frac{1}{2}$).

TABLE III. X-ray emission intensities at $\theta''=180°$ for various emission frequencies. Incident electron distributions are semi-isotropic ($\theta_2=90°$, $T_e=20$ keV, $n=\frac{1}{2}$).

$h\nu$ (keV)	$I(\theta''=180°)$ (erg/sr)
20	2.467×10^{-42}
40	5.652×10^{-43}
60	1.457×10^{-43}
100	1.125×10^{-44}

TABLE IV. X-ray emission intensities at $\theta''=180°$ for various emission frequencies. Electrons are all incident at 45° with respect to the target normal ($T_e=20$ keV, $n=0$).

$h\nu$ (keV)	$I(\theta''=180°)$ (erg/sr)
20	1.08×10^{-42}
40	1.744×10^{-43}
60	3.578×10^{-44}
100	2.04×10^{-45}

D. Interpretation of measured x-ray anisotropies

We study the behavior of the hard-x-ray angular distribution when the laser irradiance is increased from 5×10^{12} W cm^{-2} to 5×10^{13} W cm^{-2}. We use thick plastic targets and are able to determine the angular distribution of electrons using the previously calculated results of Sec. III B.

First, we note (Fig. 9) that the x-ray emission presents a very good azimuthal symmetry. Figure 10 shows the experimental and theoretical polar angle x-ray distributions at low and high irradiances for $h\nu=30$ keV. The theoretical predictions are represented by the hatched regions as explained in Sec. III C. At a given irradiance, the parameters A and T_e of the distribution given by Eq. (5) are inferred by fitting the experimental x-ray spectra taken at $\theta''=45°$ with calculated angular integrated x-ray spectra given by (in erg/keV)

$$\frac{dE}{dh\nu}=\int_{h\nu}^{\infty}f(E_1)\left[\int_{h\nu}^{E_1}\frac{I_2(h\nu,E)}{dE/dx}dE\right]dE_1\ , \tag{9}$$

where dE/dx is the mean electron energy loss per unit path length, which can be approximated by the expression[27] $dE/dx=aE^{-b}$, a and b being constants for a given material (for polystyrene one has $a=1.185\times10^5$ keV$^{1.72}$cm^{2}g^{-1} and $b=0.72$). $I_2(h\nu,E)$ [from Eq. (2)] is the thin-target emission integrated over all angles given for low-Z targets such as plastic ($Z=3.5$). A correction factor which takes into account the anisotropy of x-ray emission is also introduced.

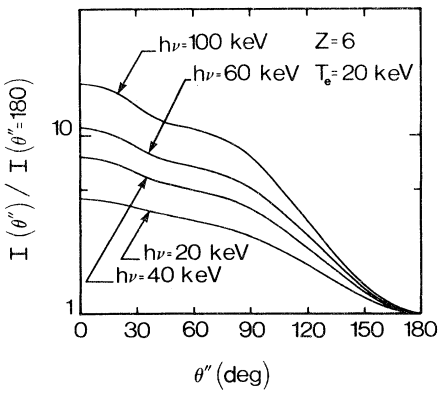

FIG. 8. Normalized angular x-ray distributions for various emission frequencies. Electrons are all incident at 45° with respect to the target normal ($T_e=20$ keV, $n=0$).

From Fig. 10 one sees that, at low irradiance, the x-ray angular distribution calculated for normal electron incidence is in very good agreement with the experimental results. At $I_L\geq10^{13}$ W cm^{-2}, the electrons no longer have an incidence normal to the target; a semi-isotropic angular distribution of hot electrons has to be used to calculate an anisotropy which agrees with the experimental values. The same type of results are also obtained for other x-ray energies. Figure 11 shows the behavior of the ratio of x-ray emission at $\theta''=110°$ to the emission at $\theta''=180°$ as a function of laser irradiance. When I_L increases, one sees that the experimental values decrease faster than the calculated predictions performed with electrons at normal incidence. The incident electron source, spatially integrated over the target surface, becomes semi-isotropic at $I_L\geq3\times10^{13}$ W cm^{-2}.

IV. HOT-ELECTRON PENETRATION

In this section we will demonstrate the importance of the direction of incidence of hot electrons for the determination of axial transport properties. By comparing calculated continuum x-ray spectra as well as energy-deposition profiles with experimental results, we show the influence of the angular distribution of hot electrons on axial deposition characteristics and we corroborate the conclusions derived above on the dependence of the angular distribution of hot electrons upon irradiance.

The axial transport properties are inferred from the substrate hard-x-ray continuum emitted by the hot electrons after being decelerated in plastic. The inward resolution is obtained with increasing thickness of low-Z plastic deposited on a gold substrate. The x-ray emission I_g from the gold only, is obtained by using the relation

$$I_g/I_0=[1-C(I_t/I_0)](1-C)^{-1}\ , \tag{10}$$

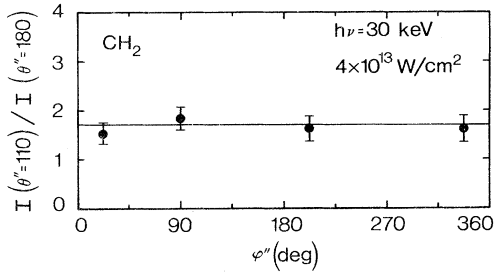

FIG. 9. Azimuthal variation of the experimental hard-x-ray emission ($h\nu=30$ keV).

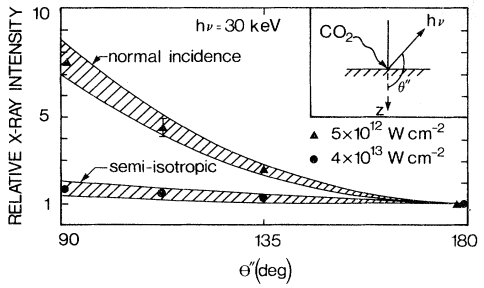

FIG. 10. Experimental and theoretical angular x-ray distributions ($h\nu=30$ keV) emitted from a thick plastic target. A perpendicular source of incident electrons with $T_e=11$ keV and $n=\frac{1}{2}$ gives the best fit to the data at low irradiance. A semi-isotropic source, with $T_e=17$ keV and $n=\frac{1}{2}$, is required at high irradiance. Hatched region for the theoretical predictions reflects the uncertainty due to scattering and energy losses of the electrons in the solid plastic.

where I_t is the total x-ray emission, C is the contrast defined as the ratio between the emission from bare gold (I_0) and a thick plastic material.

A. Low laser irradiance (5×10^{12} W/cm^2)

A theoretical x-ray spectrum is obtained by calculating the emission of the gold tracer under the bombardment of electrons transmitted through a layer of plastic. A simple approach can be taken for normal incidence and low-Z material such as plastic.

The energy distribution $g(E)$ transmitted through a layer of material of thickness x can be related to the incident distribution $f(E_1)$ by the expression

$$g(E)=T\left[\frac{x}{R}\right]\left[1-\frac{s}{R}\right]^{b/(1+b)} f(E_1)\ , \tag{11}$$

where R is the electron range which is closely approximated by the expression[27] $R=E_1^{1+b}/a(1+b)$. The parameter s is the actual path length of an electron in the material of thickness x. In plastic, $s\sim x$ is a good approximation for the electrons.[28] E is the energy of an electron of initial energy E_1 which has traveled a distance s in the plastic. E is approximated by the expression $E=E_1(1-s/R)^{1/(1+b)}$.

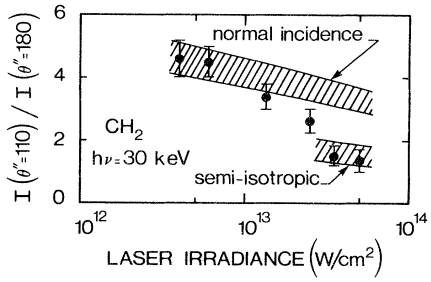

FIG. 11. Variation of the normalized emission at $\theta=110°$ with the laser irradiance, for a thick plastic target. Results calculated for a normal incidence (with a law $T_e\sim I_L^{1/4}$) and for a semi-isotropic incidence of electrons are represented by hatched regions which reflect the uncertainty due to scattering and energy losses of the electrons in the solid plastic.

$T(x/R)$ is the electron transmission law, which in the case of normal incidence on plastic is given by the semiempirical relation[29]

$$T(x/R)=1.29(1-x/R)^{1.16}-0.29(1-x/R)^{4.77}\ . \tag{12}$$

The emission in the gold tracer is calculated with inclusion of the electron backscattering losses. The x-ray spectrum is the sum of the emission due to absorbed electrons (in erg/keV)

$$\left.\frac{dE}{dh\nu}\right|_{\rm abs}=\int_{h\nu}^{\infty}(1-\eta)g(E)\left[\int_{h\nu}^{E}\frac{I'(h\nu,E')}{dE'/dx}dE'\right]dE\ , \tag{13a}$$

and backscattered electrons (in erg/keV)

$$\left.\frac{dE}{dh\nu}\right|_{\rm back}=\int_{h\nu}^{\infty}\eta g(E)\left[\int_{\xi}^{E}\frac{I'(h\nu,E')}{dE'/dx}dE'\right]dE\ . \tag{13b}$$

For high-Z targets,

$$I'(h\nu,E')=8n_ie^6Z^2G(h\nu,E')/3hmc^3E'\ ,$$

where $G(h\nu,E')$ is the Gaunt factor taken in the Born approximation.[30] The fraction η of the incident electrons backscattered from a thick gold target is nearly independent of E and has a value of 0.5. The backscattered electrons travel only a small distance in gold and come out with an energy $E_s=0.75E$. The integration limit ξ is $\max(h\nu,E_s)$. The effective Z seen by an electron along its path depends on the energy of the electron; it is estimated[25] with the Thomas-Fermi model of the atom.

The photon reabsorption in the gold substrate is estimated to be about 20% for low-energy photons ($\sim$20 keV) and negligible for more-energetic photons. In order to obtain the spectra at the angle of experimental observation and since the calculated spectra is integrated over all

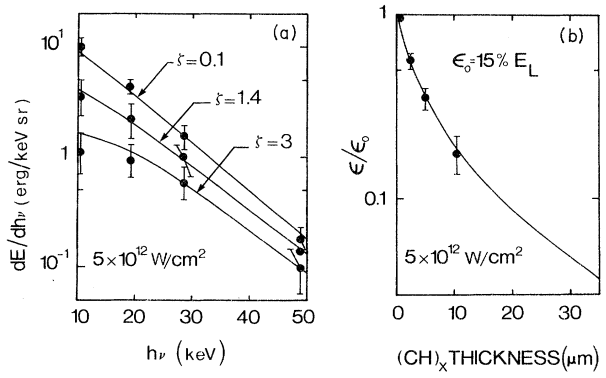

FIG. 12. Multilayer target results at low irradiance (5×10^{12} W/cm^2). (a) Experimental (points) and theoretical (solid lines) hard-x-ray continuum spectra; ζ is the plastic thickness normalized to the range calculated for the hot-electron temperature: $\zeta=x/R(T_e)$ with $R(T_e)=3.5$ μm. (b) Experimental (points) and theoretical (solid line) values of transmitted energies by various plastic layers. In (a) and (b) calculated results are obtained for electrons at normal incidence (with $n=\frac{1}{2}$).

angles, we use an anisotropy correction factor deduced from emission data[18,26] for high-Z targets bombarded by monoenergetic electrons. Figure 12(a) presents the theoretical spectra calculated with the incident distribution as given in Sec. III D ($A=2\times10^{12}$ keV$^{-3/2}$, $kT_e=11$ keV, $n=\frac{1}{2}$). The experimental spectra are in very good agreement with the calculations.

The axial hot-electron energy-deposition profile is presented in Fig. 12(b). The theoretical curve which gives the transmitted energy ϵ through a CH layer of thickness x is derived from Eqs. (11) and (12). The incident distribution is given by Eq. (5). We have

$$\epsilon/\epsilon_0=\int_\phi^\infty \frac{y^{n+1}f(y,x)e^{-y}dy}{\Gamma(n+2)} ,$$
$$\phi=[x/R(T_e)]^{0.58},\quad R(T_e)=\frac{(kT_e)^{1.72}}{a(1+b)} ,$$
$$y=E_1/kT_e , \tag{14}$$
$$f(x,y)=1.29\left[1-\frac{x}{y^{1.72}R(T_e)}\right]^{1.74}$$
$$-0.29\left[1-\frac{x}{y^{1.72}R(T_e)}\right]^{5.35} ,$$

where $\epsilon_0=\epsilon(x=0)$ is the total energy deposited inward by hot electrons.

Data on transmitted energy are obtained by integrating $Eg_{\text{expt}}(E)$ where $g_{\text{expt}}(E)$ is the experimental electron energy distribution obtained below various plastic depths. This distribution is found by fitting axially resolved experimental spectra such as those of Fig. 12(a) with bremsstrahlung emission calculations [Eq. (13)], involving $g_{\text{expt}}(E)$.

A very good agreement is found between the predictions of the model and the experimental results. This corroborates the conclusions derived from x-ray angular distribution, that the energetic electrons are normally incident at low laser irradiance.

B. High laser irradiance (4×10^{13} W cm^{-2})

The theoretical x-ray spectra of the gold tracer at high irradiance can be simply obtained only in the case of normal incidence since the transmission law $T(x)$ is not analytically known for other angular distributions. As a point of comparison, we can calculate the tracer spectra

$$\psi(x/R(T_e))=\int_{\phi'(x/R(T_e))}^\infty y^{-0.22}e^{-y}\left[1-\left[\frac{\phi'(x/R(T_e))}{y}\right]^{1.72}\right]dy ,$$
$$\phi'(x/R(T_e))=[1.24x/R(T_e)]^{0.58} .$$

For the normal-incidence curve we use the analytical model of Sec. IV A.

The experimental values agree very well with the predictions of the semi-isotropic model. This conclusion is in complete agreement with the x-ray angular distribution results.

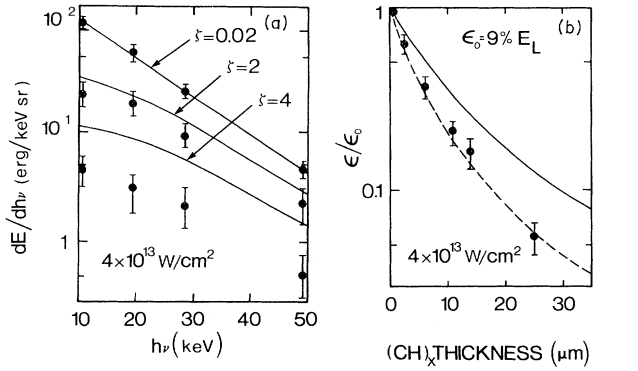

FIG. 13. Multilayer target results at high irradiance (4×10^{13} W/cm^2). (a) Experimental (points) and calculated (solid lines, obtained for electron normal indicence) hard-x-ray specta; ζ is the plastic thickness normalized to the range calculated for the hot-electron temperature: $\zeta=x/R(T_e)$ with $R(T_e)=6$ μm. (b) Experimental (points) and theoretical values of transmitted energies by various plastic layers. Solid and dashed lines are, respectively, for a normal and a semi-isotropic incidence.

under various plastic layers at normal incidence following the same procedure as described in Sec. IV A, with an initial distribution at high irradiance obtained as explained in Sec. III D ($A=3.6\times10^{12}$ keV$^{-3/2}$, $kT_e=17$ keV, $n=\frac{1}{2}$). The results are shown in Fig. 13(a). There is a difference between calculated and measured spectra as the plastic thickness is increased, indicating clearly that at high irradiance the incident distribution is no longer normal to the target surface.

Figure 13(b) shows the fraction of incident hot-electron energy transmitted below various plastic thicknesses at 4×10^{13} W cm^{-2}. The solid lines are theoretical calculations with two types of electron angular distributions (normal and semi-isotropic) and the same energy distribution $f(E_1)=AE_1^{1/2}\exp(-E_1/kT_e)$. The energy-deposition curve in the planar semi-isotropic case is obtained by using the electron transport calculations of Spencer.[31,32] In this case the fraction of incident energy transmitted through a CH layer of thickness x is

$$\epsilon/\epsilon_0=1-\frac{\int_0^{x/R(T_e)}\psi(x/R(T_e))dx}{\int_0^\infty\psi(x/R(T_e))dx} \tag{15}$$

with[33]

V. CONCLUSION

We have shown that the hot electrons which are reflected at the plasma cloud boundary and come back on the target are characterized by an *energy* distribution as well as by a *directional* distribution. In this paper, emphasis

has been put on the calculation of the hard-x-ray angular distribution and on the determination of the spatially averaged directional distribution of incident hot electrons at various irradiances. The importance of this directional distribution in regards to axial transport has also been analyzed in detail by means of a comparison between experimental hard-x-ray spectra and theoretical models.

Different types of spatially integrated directional distribution of hot electrons can be simply related to the existence of induced magnetic fields, since the presence of such fields will affect the trajectories of the electrons. At low irradiance, in the presence of weak magnetic fields, incident hot electrons will have near-normal incidence. At high irradiance with stronger magnetic fields, electrons will be more easily radially convected and will penetrate into the target in a manner which involves a considerable distribution of angles of incidence. Spatially averaged features of the electron distribution at high irradiance are also consistent with a small fraction of the electrons at normal incidence near the focal spot and most of the electrons being incident at oblique angles away from the focal spot.[11] A precise knowledge of the direction of incidence of hot electrons gives an important insight in the physics of the laser-matter interaction and allows a quantitative determination of hot-electron energy deposition.

ACKNOWLEDGMENTS

The authors acknowledge useful discussions with T. W. Johnston, P. Lavigne, F. Martin, B. Terreault, and F. Amiranoff. The continuing excellent technical support of J. Gauthier, P. P. Mercier, F. Poitras, and J. G. Vallée is also quite appreciated. This research was supported in part by the Natural Sciences and Engineering Research Council of Canada.

[1]K. B. Mitchel and R. P. Godwin, J. Appl. Phys. 48, 3851 (1977).

[2]J. C. Kieffer, H. Pépin, F. Martin, P. Church, T. W. Johnston, and R. Décoste, Phys. Rev. Lett. 44, 1128 (1980).

[3]J. Hares, J. Kilkenny, M. M. Key, and J. G. Lunmey, Phys. Rev. Lett. 42, 1216 (1979).

[4]R. S. Marjoribanks, M. D. J. Burgess, G. D. Enright, and M. C. Richardson, Phys. Rev. Lett. 45, 1798 (1980).

[5]R. Décoste, J. C. Kieffer, and H. Pépin, Phys. Rev. Lett. 47, 35 (1981).

[6]F. Amiranoff, K. Eidman, R. Sigel, R. Fedosejevs, A. Maaswinkel, Yung Lee Teng, J. D. Kilkenny, J. D. Hares, D. K. Bradley, B. J. MacGowan, and T. J. Goldsack, J. Phys. D 15, 2463 (1982).

[7]N. A. Ebrahim, C. Joshi, and H. A. Baldis, Phys. Rev. A 25, 2440 (1982); N. H. Burnett *et al.*, in *Japan-U.S. Seminar on Theory and Application of Multiply Ionized Plasmas Produced by Laser and Particle Beams, Nara, 1982,* edited by C. Yamanaka (Osaka University, Osaka, 1982).

[8]R. Decoste, J. C. Kieffer, M. Piché, H. Pépin, and P. Lavigne, Phys. Fluids 25, 1699 (1982).

[9]D. W. Forslund and J. U. Brackbill, Phys. Rev. Lett. 48, 1614 (1982); R. Fabbro and P. Mora, Phys. Lett. 90A, 48 (1982).

[10]M. A. Yates, D. B. Van Hulsteyn, H. Rutkowsky, G. Kyvala, and J. U. Brackbill, Phys. Rev. Lett. 49, 1702 (1982).

[11]J. C. Kieffer, H. Pépin, M. Piché, J. P. Matte, T. W. Johnston, P. Lavigne, F. Martin, and R. Décoste, Phys. Rev. Lett. 50, 1054 (1983).

[12]C. E. Max, in *Laser-Plasma Interaction, Les Houches Lectures, 1980,* edited by R. Balian and J. C. Adam (North-Holland, Amsterdam, 1982).

[13]F. C. Young, Phys. Rev. Lett. 33, 767 (1974); K. Eidmann, M. H. Key, and R. Sigel, J. Appl. Phys. 47, 2402 (1976); O. N. Krokhin, Yu. A. Mikhailov, U. V. Pustovalov, A. A. Rupasov, V. P. Silin, G. Sklizkov, and A. S. Shikanov, Zh. Eksp. Teor. Fiz. 69, 206 (1975) [Sov. Phys.—JETP 42, 107 (1975)]; V. Blazhenkov, A. N. Kirkin, A. V. Kononov, L. P. Kotenko, A. M. Leontovich, G. I. Merzon, A. M. Mozharovsky, and S. D. Zakharov, Opt. Commun. 34, 231 (1980).

[14]K. Eidmann, Plasma Phys. 17, 121 (1975).

[15]A. Sommerfeld, Ann. Phys. (Leipzig) 11, 257 (1931).

[16]H. Pépin, F. Martin, B. Grek, T. W. Johnston, J. C. Kieffer, and G. Mitchel, J. Appl. Phys. 50, 6784 (1979).

[17]H. K. Tseng, R. H. Pratt, and C. M. Lee, Phys. Rev. A 1, 528 (1970); C. M. Lee, L. Kissel, R. H. Pratt, and H. K. Tseng, *ibid.* 13, 1714 (1976).

[18]H. K. Tseng, R. H. Pratt, and C. M. Lee, Phys. Rev. A 19, 187 (1979).

[19]H. Kulenkampff, M. Scheer, and E. Zeitler, Z. Phys. 157, 275 (1959).

[20]D. H. Rester, N. Edmonson, and Q. Peasley, Phys. Rev. A 2, 2190 (1970).

[21]R. Weinstock, Phys. Rev. 61, 548 (1942).

[22]G. Elwert, Ann. Phys. (Leipzig) 34, 178 (1939); G. Elwert and E. Hang Phys. Rev. 183, 90 (1969).

[23]T. E. Everhart, J. Appl. Phys. 31, 1483 (1960).

[24]V. E. Cosslett and R. N. Thomas, Br. J. Appl. Phys. 15, 883 (1964); H. E. Bishop, Proc. Phys. Soc. London 85, 855 (1965).

[25]J. C. Kieffer, Ph.D. thesis, Université du Québec, 1982.

[26]J. G. Chervenak and A. Liuzzi, Phys. Rev. A 12, 26 (1975).

[27]M. Berger, S. Seltzer, U.S. National Aeronautics and Space Administration Report No. NASA-SP3012, 1964 (unpublished).

[28]For polystyrene, we find a very good agreement between our model and Spencer calculations (difference less than 10%) when $x/R \leq 0.7$.

[29]C. Zeller and J. Ruste, Rev. Phys. Appl. 4, 441 (1976).

[30]I. P. Shkarofsky, T. W. Johnston, and M. P. Bachinsky, *The Particle Kinetics of Plasmas* (Addison-Wesley, Reading, Mass., 1966).

[31]L. V. Spencer, Phys. Rev. 98, 1597 (1955); U.S. Natl. Bur. Stand. Monograph No. 1 (U.S. GPO, Washington, D.C., 1959).

[32]R. J. Harrach and R. E. Kidder, Phys. Rev. A 23, 887 (1981).

[33]$\psi(x/R(T_e))$ can be closely approximated by the functional form $\exp\{-1.9[x/R(T_e)]^{1/2}\}$.